

# Microspotting Streptavidin and Double-Stranded DNA Arrays on Gold for High-Throughput Studies of Protein–DNA Interactions by Surface Plasmon Resonance Microscopy

Jennifer S. Shumaker-Parry,<sup>†,‡</sup> M. Hadi Zareie,<sup>†,§</sup> Ruedi Aebersold,<sup>||</sup> and Charles T. Campbell<sup>\*,†</sup>

Department of Chemistry, University of Washington, Seattle, Washington 98195-1700, and Institute for Systems Biology, 1441 North 34th Street, Seattle, Washington 98103

**We present two strategies for microspotting  $10 \times 12$  arrays of double-stranded DNAs (dsDNAs) onto a gold-coated glass slide for high-throughput studies of protein–DNA interactions by surface plasmon resonance (SPR) microscopy. Both methods use streptavidin (SA) as a linker layer between a biotin-containing mixed self-assembled monolayer (SAM) and biotinylated dsDNAs to produce arrays with high packing density. The primary mixed SAM is produced from biotin- and oligo(ethylene glycol)-terminated thiols bonded as thiolates onto the gold surface. In the first method, a robotic microspotter is used to deliver nanoliter droplets of dsDNA solution onto a uniform layer of this SA ( $\sim 2 \times 10^{12}$  SA/cm<sup>2</sup>). SPR microscopy shows a density of  $(5–6) \times 10^{11}$  dsDNA/cm<sup>2</sup> ( $0.2–0.3$  dsDNA/SA) in the array elements. The second method uses instead a microspotted array of this SA linker layer, onto which the microspots of dsDNA are added with spatial registry. SPR microscopy before addition of the dsDNA shows a SA coverage of  $2 \times 10^{12}$  SA/cm<sup>2</sup> within the spots and a dsDNA density of  $8.5 \pm 3.5 \times 10^{11}$  dsDNA/cm<sup>2</sup> ( $0.3–0.7$  dsDNA/SA, depending on the length of dsDNA) after dsDNA spotting. We demonstrate the ability to simultaneously monitor protein binding with the SPR microscope in many 200- $\mu$ m spots with 1-s time resolution and sensitivity to  $< 1$  pg of protein.**

The advantages provided by microarray analysis of interactions between biomolecules are many. Parallel, high-throughput monitoring of binding between biomolecules has important implications in medical research and diagnostics,<sup>1–6</sup> drug discovery,<sup>7–9</sup> funda-

mental molecular and cellular biology investigations,<sup>10–12</sup> and analytical sensor development.<sup>13–17</sup>

Surface plasmon resonance (SPR) microscopy is a promising tool for quantitative, real-time monitoring of biomolecule interactions taking place over a relatively large area of a sensing surface without the need for labeling.<sup>18–24</sup> Recently, SPR microscopy (also called “imaging SPR”) has been used to study biomolecule interactions in a parallel fashion by creating an array of binding sites on a sensor surface and monitoring adsorption of biomolecules to those sites.<sup>23,25–31</sup> Real-time quantitative measurement

\* Corresponding author. E-mail: campbell@chem.washington.edu. Fax: 206-616-6250.

<sup>†</sup> University of Washington.

<sup>‡</sup> Current address: Max-Planck-Institut für Polymerforschung, Ackermannweg 10, D-55128 Mainz, Germany.

<sup>§</sup> Current address: Institute for Nanoscale Technology, University of Technology, P.O. Box 123, Broadway NSW, Sydney, Australia 2007.

<sup>||</sup> Institute for Systems Biology.

(1) Young, R. A. *Cell* **2000**, *102*, 9–15.

(2) Epstein, C. B.; Butow, R. A. *Curr. Opin. Biotechnol.* **2000**, *11*, 36–41.

(3) Rhodes, D. R.; Chinnaiyan, A. M. *J. Invest. Surg.* **2002**, *15*, 275–279.

(4) Tefferi, A.; Bolander, M. E.; Ansell, S. M.; Wieben, E. D.; Spelsberg, T. C. *Mayo Clin. Proc.* **2002**, *77*, 927–940.

(5) Haupl, T.; Burmester, G. R.; Stuhlmüller, B. *Z. Rheumatologie* **2002**, *61*, 364–404.

(6) Faber, B. C. G.; Heeneman, S.; Daemen, M. J. A. P.; Cleutjens, K. B. *Curr. Opin. Lipid.* **2002**, *13*, 545–552.

(7) Lal, S. P.; Chrisopherson, R. I.; dos Remedios, C. G. *Drug Discovery Today* **2002**, *7*, S143–S149.

(8) Courtneidge, S. A.; Plowman, G. D. *Curr. Opin. Biotechnol.* **1998**, *9*, 632–636.

(9) Braxton, S.; Bedilion, T. *Curr. Opin. Biotechnol.* **1998**, *9*, 643–649.

(10) Zhu, H.; Bilgin, M.; Bangham, R.; Hall, D.; Casamayor, A.; Bertone, P.; Lan, N.; Jansen, R.; Bidlingmaier, S.; Houfek, T.; Mitchell, T.; Miller, P.; Dean, R. A.; Gerstein, M.; Snyder, M. *Science* **2001**, *293*, 2101–2105.

(11) MacBeath, G.; Schriber, S. L. *Science* **2000**, *289*, 1760–1763.

(12) Heller, M. J. *Annu. Rev. Biomed. Eng.* **2002**, *4*, 129–153.

(13) Rowe, C. A.; Tender, L. M.; Feldstein, F. J.; Golden, J. P.; Scruggs, S. B.; MacCraith, B. D.; Cras, J. J.; Ligler, F. S. *Anal. Chem.* **1999**, *71*, 3846–3852.

(14) Cho, E. J.; Tao, Z.; Tehan, E. C.; Bright, F. V. *Anal. Chem.* **2002**, *74*, 1462–1466.

(15) Lavigne, J. J.; Savoy, S.; Clevenger, M. B.; Ritchie, J. E.; McDoniel, B.; Yoo, S.-J.; Anslin, E. V.; McDevitt, J. T.; Shear, J. B.; Neikirk, D. *J. Am. Chem. Soc.* **120**, 6429–6430.

(16) Christodoulides, N.; Tran, M.; Floriano, P. N.; Rodriguez, M.; Goodey, A. *Anal. Chem.* **2002**, *74*, 3030–3036.

(17) Michael, K. L.; Taylor, L. C.; Schultz, S. L.; Walt, D. R. *Anal. Chem.* **1998**, *70*, 1242–1248.

(18) Rothenhausler, B.; Knoll, W. *Nature* **1988**, *332*, 615–617.

(19) Zizlsperger, M.; Knoll, W. *Prog. Colloid Polym. Sci.* **1998**, *109*, 244–253.

(20) Aust, E. F.; Sawodny, M.; Ito, S.; Knoll, W. *Scanning* **1994**, *16*, 353–361.

(21) Knoll, W. *Annu. Rev. Phys. Chem.* **1998**, *49*, 569–638.

(22) Berger, C. E. H.; Beumer, T. A. M.; Kooyman, R. P. H.; Greve, J. *Anal. Chem.* **1998**, *70*, 703–706.

(23) Thiel, A. J.; Frutos, A. G.; Jordan, C. E.; Corn, R. M.; Smith, L. M. *Anal. Chem.* **1997**, *69*, 4948–4956.

(24) Lyon, L. A.; Holliday, W. D.; Natan, M. J. *Rev. Sci. Instrum.* **1999**, *70*, 2076–2081.

(25) Li, M.; Lee, H. J.; Condon, A. E.; Corn, R. M. *Langmuir* **2002**, *18*, 805–812.

(26) Guedon, P.; Livache, T.; Martin, F.; Lesbire, F.; Roget, A.; Bidan, G.; Levy, Y. *Anal. Chem.* **2000**, *72*, 6003–6009.

(27) Jordan, C. E.; Corn, R. M. *Anal. Chem.* **1997**, *69*, 1449–1456.

of adsorption and desorption events using an SPR microscope is possible when reflected light intensity is monitored at a high-contrast angle near the SPR minimum.<sup>19,32,33</sup> Changes in reflected light intensity monitored at such a high-contrast angle can be converted to real-time changes in effective refractive index, effective adlayer thicknesses, and absolute surface coverages of molecules using methods described in ref 33. These methods are based on the extension of formulas developed for quantitation of SPR spectroscopy data (SPR angle or wavelength shifts) and rely on a simple calibration of the SPR microscope's response to changes in bulk solutions' refractive index.<sup>33,34</sup> Such quantitative SPR microscopy measurements are important whenever interactions between biomolecules are being studied.

Protein interactions with double-stranded DNAs (dsDNAs) are of fundamental importance in biology and medicine and play a vital role in cellular processes including transcription regulation, genetic recombination, DNA repair, and the restriction and modification of DNA.<sup>35</sup> To use SPR microscopy for protein–dsDNA array analysis, a method must be developed to pattern dsDNAs on an SPR-active surface, typically a glass slide coated with a thin gold film (~50 nm). A few methods have been used to fabricate dsDNA arrays on gold. Brockman et al. used amine-terminated alkythioliates and hybridization between complementary single-stranded DNAs (ssDNAs) to create an array of dsDNAs for measuring protein–DNA interactions.<sup>31,36</sup> They observed some nonspecific binding of a ssDNA-binding protein to array elements that should contain only dsDNAs.<sup>31</sup> Smith et al. used this same technique to create an array of dsDNAs.<sup>37</sup> Incomplete hybridization for a 38-base pair ssDNA was explained by possible accessibility problems due to nonspecific interactions of the immobilized ssDNA with the surface or formation of secondary structure.<sup>37</sup>

O'Brien et al. prepared an array of dsDNAs on a gold surface for atomic force microscopy studies of protein–dsDNA interactions<sup>38,39</sup> by depositing disulfide-modified dsDNAs onto bare gold regions created by photopatterning. One drawback of this method is the potential for nonspecific interactions of dsDNA with bare gold, which may be why they observed smaller than expected heights for some array elements.<sup>39</sup> Since alkythioliates often self-segregate in mixed monolayers on Au, this method could give a very nonuniform distribution of dsDNAs on the surface.<sup>40</sup>

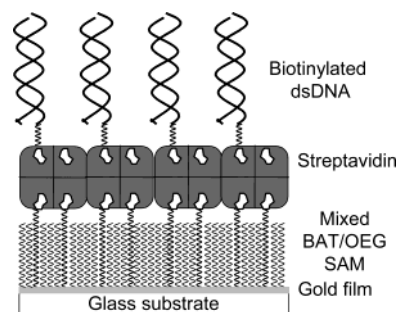


Figure 1. Idealized cartoon of biotinylated double-stranded DNA immobilized on a SA monolayer. This protein layer is adsorbed on a mixed BAT/OEG binary alkythiolate monolayer. The biotin moiety of the biotinylated surface thiolate inserts ~14 Å into the SA binding pocket leading to the formation of a nearly close-packed monolayer of SA on the surface. Similarly, the biotinylated dsDNA then binds via its 5'-biotin modification on this SA layer. Note that the thiol molecules are not expected to display such high order and rigid orientation; a more accurate description of the composition, orientation, and order within these mixed monolayers is presented elsewhere.<sup>46</sup> No attempt is made to show the known tilting of the alkyl chains. Not drawn to scale.

To measure protein–dsDNA interactions on a planar surface, the dsDNAs must be accessible (not too tightly packed) so the protein or protein complex is able to recognize its DNA binding site and have space to bind. Ideally, this spacing would be optimized without significantly decreasing binding signals. One major challenge in using the dsDNA immobilization strategies mentioned above is the difficulty in controlling the minimum spacing between dsDNAs. Each of those methods could result in closely packed DNA-rich regions displaying no or weak, nonspecific binding of proteins, complicating array analysis. Trying to overcome this problem, we recently used a streptavidin (SA) linker layer to immobilize biotinylated dsDNAs on a planar gold surface with high density ( $(1-3) \times 10^{12}$  DNA/cm<sup>2</sup>, depending on the dsDNA length) and adequate spacing (~4 nm closest possible DNA–DNA separation at the surface) for the binding of proteins.<sup>41</sup> This method is shown schematically in Figure 1. The SA monolayer, which offers  $\sim 5 \times 10^{12}$  biotin sites/cm<sup>2</sup>, was prepared first by adsorbing SA onto a mixed self-assembled monolayer (SAM) on gold, which contained biotin- and oligo(ethylene glycol)-terminated alkythioliates (BAT and OEG, respectively). Figure 2 shows the chemical structures of BAT and OEG. Oligo(ethylene glycol) is used as a headgroup on the OEG and as a spacer in the BAT because it resists nonspecific protein adsorption<sup>42-46</sup> and nonspecific DNA adsorption<sup>42</sup> to the surface. For the proper thiol mixture, the biotin headgroups allow the specific immobilization of SA to the SAM surface, reaching a packing density within ~20% of that for a crystalline SA monolayer grown at the air–water

(28) Nelson, B. P.; Frutos, A. G.; Brockman, J. M.; Corn, R. M. *Anal. Chem.* **1999**, *71*, 3928–3934.

(29) Nelson, B. P.; Grimsrud, T. E.; Liles, M. R.; Goodman, R. M.; Corn, R. M. *Anal. Chem.* **2001**, *73*, 1–7.

(30) Frutos, A. G.; Brockman, J. M.; Corn, R. M. *Langmuir* **2000**, *16*, 2192–2197.

(31) Brockman, J. M.; Frutos, A. G.; Corn, R. M. *J. Am. Chem. Soc.* **1999**, *121*, 8044–8051.

(32) Shumaker-Parry, J. S.; Nelson, K. E.; Aebersold, R.; Campbell, C. T. In preparation.

(33) Shumaker-Parry, J. S.; Campbell, C. T. *Anal. Chem.* **2004**, *76*, 907–917.

(34) Jung, L. S.; Campbell, C. T.; Chinowsky, T. M.; Mar, M. N.; Yee, S. S. *Langmuir* **1998**, *14*, 5636–5648.

(35) Guille, M. J.; Kneale, G. G. *Mol. Biotechnol.* **1997**, *8*, 35–52.

(36) Brockman, J. M.; Nelson, B. P.; Corn, R. M. *Annu. Rev. Phys. Chem.* **2000**, *51*, 41–63.

(37) Smith, E. A.; Erickson, M. G.; Ulijasz, A. T.; Weisblum, B.; Corn, R. M. *Langmuir* **2002**, *17*, 1486–1492.

(38) O'Brien, J. C.; Stickney, J. T.; Porter, M. D. *J. Am. Chem. Soc.* **2000**, *122*, 5004–5005.

(39) O'Brien, J. C.; Stickney, J. T.; Porter, M. D. *Langmuir* **2000**, *16*, 9559–9567.

(40) Stranick, S. J.; Parikh, A. N.; Tao, Y.-T.; Allara, D. L.; Weiss, P. S. *J. Phys. Chem.* **1994**, *98*, 7636–7646.

(41) Shumaker-Parry, J. S.; Campbell, C. T.; Stormo, G. D.; Silbaq, F. S.; Aebersold, R. H. *Proc. SPIE: Scanning and Force Microscopies for Biomedical Applications II*; San Jose, CA, 2000; pp 158–166.

(42) Bambdad, C. *Biophys. J.* **1998**, *75*, 1997–2003.

(43) Jung, L. S.; Nelson, K. E.; Campbell, C. T.; Stayton, P. S.; Yee, S. S.; Perez-Luna, V.; Lopez, G. P. *Sens. Actuators, B* **1999**, *54*, 137–144.

(44) Prime, K. L.; Whitesides, G. M. *J. Am. Chem. Soc.* **1993**, *115*, 10714–10721.

(45) Pale-Grosdemange, C.; Simon, E. S.; Prime, K. L.; Whitesides, G. M. *J. Am. Chem. Soc.* **1991**, *113*, 12–20.

(46) Nelson, K. E.; Gamble, L.; Jung, L. S.; Boeckl, M. S.; Naeemi, E.; Golledge, S. L.; Sasaki, T.; Castner, D. G.; Campbell, C. T.; Stayton, P. S. *Langmuir* **2001**, *17*, 2807–2816.

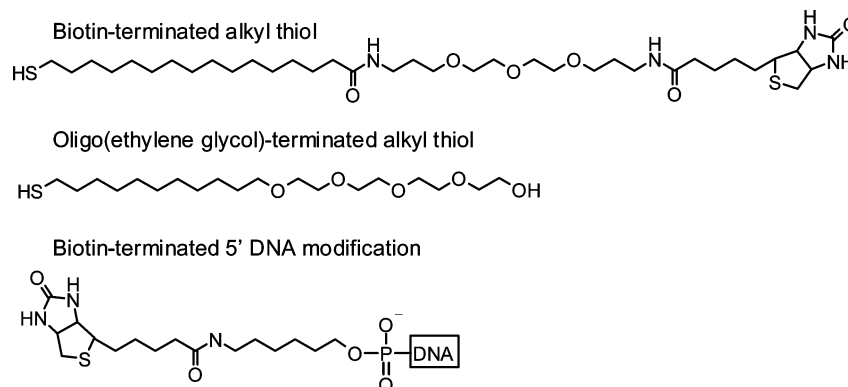


Figure 2. Bond-line structures of the thiols used in the mixed SAM and the biotin/linker functionality that is covalently attached to the 5' end of one strand of the dsDNA for immobilization via a streptavidin linker layer.

interface.<sup>47</sup> The immobilized SA provides a very stable monolayer with an estimated half-life in excess of 100 days even with excess biotin in solution.<sup>43</sup> One strand of the dsDNA is functionalized on its 5' end with the biotin linker shown in Figure 2. The spacer between the DNA and the biotin provides flexibility and spacing so that the biotin tail group can fit into its binding pocket in the SA. The dsDNA-functionalized surface was shown to resist nonspecific protein adsorption and was used to measure the specific binding of a dsDNA-binding protein to its binding site immobilized on the surface.<sup>41</sup>

In this paper, we describe an application of this SA linker layer to immobilize dsDNAs by microspotting them in an array. We also describe a method for microspotting the SA itself to form this linker layer and its application for microspotting dsDNA arrays. Successful application of the resulting SA and dsDNA arrays for simultaneously studying protein–DNA interactions with different sequences of dsDNA by SPR microscopy is described elsewhere.<sup>48</sup>

Others groups have fabricated a SA array on a gold surface. Zizlsperger and Knoll patterned a mixed SAM containing biotin- and OH-terminated alkanethiolates onto a bare gold surface using an ink jet printing technique.<sup>19</sup> One potential problem with this method is the ability to form a high-quality SAM that will resist nonspecific DNA and protein adsorption. The adsorption time (~2 h) for the thiols is short compared to that generally used for SAM formation (12–24 h). Longer adsorption times are usually necessary to form a well-ordered, close-packed SAM.<sup>49</sup> Zizlsperger and Knoll did not present results characterizing the nonspecific binding of protein or DNA to their surfaces.

Riepl et al.<sup>50</sup> also prepared a SA array on a surface prefunctionalized with a SAM of biotin- and OEG-terminated thioliates. The SAM was formed on a commercial chip (XNA on Gold) that contained a pattern of bare gold spots surrounded by Teflon. SA was adsorbed from solution to these spots, and then biotinylated ssDNA was spotted onto the SA spots (diameter, 1.5 mm). The maximum SA packing density on their mixed SAM was ap-

proximately half that we typically achieve (see below). Riepl et al. attributed the low SA packing density to a decreased accessibility of the biotin headgroup to the SA due to the formation of a hydrogen-bonding network between neighboring amide groups. The decreased packing density means there are fewer binding sites per square centimeter available for immobilization of biomolecules such as DNA, which could result in a lower signal during related analyses.

Here we show how dsDNA can be immobilized in a  $10 \times 12$  array of 200- $\mu\text{m}$  spots with a high packing density ( $(0.5\text{--}1.2) \times 10^{12}$  dsDNA/ $\text{cm}^2$ ) on gold using a SA linker layer whereon  $\sim 0.2\text{--}0.7$  dsDNA bind per SA, depending on the method. The ratios are consistent with that measured for similar length dsDNA adsorbed from solution to the same SA monolayer.<sup>41</sup> The microspotting process and SA linker layer described here potentially could be used to immobilize a variety of other biotinylated molecules on the same surface for flexibility in array-based studies with SPR microscopy.

## EXPERIMENTAL SECTION

**Substrate Preparation.** SPR microscope substrates ( $25 \times 35 \times 3$  mm SF14 glass slide, Schott Glass Technology, Durea, PA) were cleaned and coated with 20 Å of chromium and 475 Å of gold. Immediately before use, the gold-coated substrates were cleaned as previously described<sup>34</sup> by immersing them in basic peroxide solution at 65 °C for ~40 s. The slides were rinsed copiously with Nanopure water (18 M $\Omega$  resistivity), rinsed with absolute ethanol, and dried with nitrogen gas. Oligo(ethylene glycol)-terminated alkanethiol (OEG) was synthesized by Dr. Esmael Naeemi and provided by Prof. Buddy Ratner (University of Washington). Biotin-terminated alkanethiol (BAT) was synthesized by Dr. Maximilliane Boeckl and provided by Prof. Tomikazu Sasaki (University of Washington). These molecules are described in detail elsewhere.<sup>46</sup> The mixed SAM-functionalized surfaces were prepared as previously described.<sup>46,51</sup> In summary, a solution of 0.1 mM total thiol was prepared using a 1:9 mole ratio of BAT/OEG, in degassed absolute ethanol. The clean, gold-coated substrates were immersed in the thiol solution in a jar purged with nitrogen, sealed, and placed in the dark for 12–24 h to allow the thiols to assemble on the surface. The substrates were

(47) Darst, S. A.; Ahlers, M.; Meller, P. H.; Kubalek, E. W.; Blankenburg, R.; Ribi, H. O.; Ringsdorf, H.; Kornberg, R. D. *Biophys. J.* **1991**, *59*, 387–396.

(48) Shumaker-Parry, J. S.; Aebersold, R.; Campbell, C. T. Submitted to *Anal. Chem.*

(49) Schwartz, D. K. *Annu. Rev. Phys. Chem.* **2001**, *52*, 107–137.

(50) Riepl, M.; Enander, K.; Liedberg, B.; Schäferling, M.; Kruschina, M.; Ortiago, F. *Langmuir* **2002**, *18*, 7016–7023.

(51) Jung, L. S.; Nelson, K. E.; Stayton, P. S.; Campbell, C. T. *Langmuir* **2000**, *16*, 9421–9432.

removed from solution, rinsed liberally with absolute ethanol to remove loosely bound thiols, and dried with nitrogen. Slides that were not used immediately were placed in a covered Petri dish filled with nitrogen and sealed with Parafilm. The Petri dish was placed in a larger jar purged with nitrogen and sealed with Parafilm for long-term storage.

**DNA Preparation.** Biotinylated DNAs containing 77 base pairs (77-mer) and 100 base pairs (100-mer) were prepared from single-stranded oligonucleotides (ss-oligos) synthesized by Integrated DNA Technologies (Coraville, IA). For two complementary ss-oligos, one strand contained no modification and the other strand was synthesized with a 5'-biotin modification as shown in Figure 2. The ss-oligos were dissolved in 10 mM Tris, 10 mM NaCl, and 1 mM EDTA in Nanopure water (resistivity of 18 M $\Omega$ ) to a final concentration of 100  $\mu$ M and stored at  $-20$   $^{\circ}$ C. To prepare dsDNAs, these complementary ss-oligos were combined in equimolar ratios and annealed by immersing the sealed Eppendorf tube containing the complementary ss-oligos (one biotinylated) into a flask of boiling water and allowing the water to slowly cool to room temperature.

**Microarray Fabrication. (1) Robotic Arraying System.** The robot and software used to deliver samples to the sensor surface for microarray fabrication are part of a ChipWriter Pro robotic arraying system (Virtek Biotech, Waterloo, Canada). The system includes a water bath, a sonicator, a vacuum manifold for pin cleaning, a pin blotter station, and a 384-well microtiter plate holder. ChipWriter Pro software is used to control all aspects of robot motion. The robot controls the motion of a Stealth printhead that holds ArrayIt microspotting pins from TeleChem, International, Inc. (Sunnyvale, CA) in order to deliver a droplet of sample from each pin to the substrate surface in preselected sites on the surface. Due to the constraints of the spacing between pins in the printhead, software limitations, and a desire to minimize sample consumption, we used a single pin (SMP7, TeleChem International, Inc.) for microarray fabrication. The pin has a sample uptake volume of 250 nL and an estimated delivery volume of 1.7 nL, designed to create a spot diameter of 200–220  $\mu$ m.<sup>52</sup>

**(2) Streptavidin Immobilization in a Uniform Layer.** Streptavidin was purchased from Calbiochem (San Diego, CA) and used without further purification. Unless otherwise indicated, SA solutions were prepared at a concentration of 0.05 mg/mL in 150 mM PBS buffer at pH 7.4. SA monolayers for microarray fabrication were prepared by placing 500  $\mu$ L of SA solution on the substrate prefunctionalized with a BAT/OEG SAM. The protein was allowed to adsorb for at least 30 min in a high-humidity chamber. Then, the substrate was rinsed gently with a large volume of 150 mM PBS buffer at pH 7.4. A final rinse with water was used to remove buffer salts from the surface. A clean squirt bottle was filled with humid air from the chamber, and this air was squirted across the surface to gently remove bulk water. The substrate was used immediately for microspotting. Exposure to dry laboratory air was minimized during SA monolayer preparation.

**(3) Microspotting Process.** Prior to microspotting, 8–10  $\mu$ L of SA solution or dsDNA solution was transferred to the appropriate wells in a 384-well microtiter plate (Uniplate, 7701-5101, Whatman, Clifton, NJ). The concentrations of these solutions for

each specific microarray are included in the Results and Discussion section. The plate was covered with aluminum foil tape (1450, 3M Corp.) and a roller was used to ensure a good seal to minimize evaporation. The plate was placed in a centrifuge (Centrifuge 5810R, Eppendorf, Westbury, NY) and spun for 1 min at 2000 rotations per minute in order to ensure the solutions were at the bottom of the wells. After spinning, the tape was removed from the top of the plate before it was placed in the microtiter plate holder on the platform in the humidity-controlled chamber.

Humidity control is essential for fabricating reproducible microarrays. The humidity level determines the time allowed for adsorption of material to the functionalized surface. A relative humidity of 70% at a temperature of 24.5  $^{\circ}$ C was found to keep the surface wet for at least 2 h. When humidity dropped below 70% at this temperature, the solution deposited on the surface evaporated more quickly. For example, when the relative humidity was at 60%, the surface dried in less than 1 min. The relative humidity was maintained at 70–75% at temperatures that usually ranged from 24.5 to 25.5  $^{\circ}$ C.

Initially, the pin was cleaned by a series of immersions in the sonicator and the water bath. After each immersion, the pin was dried in the vacuum manifold. The robot then dipped the dry pin into the appropriate well of the microtiter plate to withdraw sample through capillary action. The pin moved to the blotter and tapped lightly a specified number of times on a clean, glass slide. After blotting, the robot moved the pin filled with sample to a position above the substrate on the platform. The robot brought the pin close to the substrate so the solution layer made contact with the functionalized gold-coated surface. Ideally, at this point there is no direct contact between the pin and the surface. This requires careful alignment of the arrayer platform and pin robot before use. The robot then moved the pin away from the surface, depositing a droplet of solution on the surface. Usually the robot was programmed to deposit multiple sample droplets in a row on a single substrate or on multiple substrates after each sample solution uptake. This minimizes sample volume requirements and shortens the microarray fabrication time. The center-to-center spot spacing is 450  $\mu$ m. For the arrays described in this paper, each row was made by filling the pin with a new solution from a well in the microtiter plate and the elements in a row are formed from replicate depositions from the pin after a single solution uptake. There is no reason, however, that every spot could not be functionalized with a different chemical species, but this would require longer time and a greater variety of chemicals. After depositing solutions for a row, the pin is cleaned using the process described above before filling with a new sample solution.

After spotting, the substrates were allowed to sit in the high-humidity chamber for at least 1 h to allow time for adsorption while the spot maintains a thin water film. Longer times showed no increase in sample adsorption. Then the substrate surfaces were rinsed with copious amounts of 150 mM PBS buffer at pH 7.4 and stored in that same PBS buffer at 4  $^{\circ}$ C until analysis.

When SA arrays were made, the protein was allowed to adsorb onto the mixed SAM from the spotted SA solution for at least 30 min before dsDNA was spotted onto the SA spots on the substrate. In such a process, the robot's ability to align the DNA spots with the SA spots was excellent ( $\sim$ 1  $\mu$ m). The slides were then incubated for an additional hour before rinsing with copious

(52) TeleChem International, www.arrayit.com.

amounts of PBS buffer stored as previously described. Rinsing took place in the humidity chamber, and exposure of the microarrays to dry room air was minimized.

**SPR Microscopy Measurements. (1) SPR Microscopy Image Capture and Analysis.** The microarrays were characterized using our home-built SPR microscope described and characterized in more detail elsewhere.<sup>32,33</sup> Briefly, a stabilized 632.8-nm HeNe laser serves as the excitation source for the system. The laser beam is p-polarized, expanded, and collimated before traveling through an SF14 glass hemicylindrical prism and substrate to illuminate an  $\sim 24\text{-mm}^2$  area of a gold-coated sensor surface. The detection optics are connected to an aluminum rail that is attached to a motorized rotation stage. This stage is mounted under an identical stage that holds the prism. The centers of rotation for the two stages are aligned. A computer connected to a stage controller/driver is used to separately and equally vary the angle of incidence and the angle of detection so the CCD detector stays at the specular angle for each angle of incidence. The reflected light is focused and directed by a lens directly onto the CCD detector of a video camera, creating an image that is automatically digitized by a framegrabber card (DT3155, Data Translation, Marlboro, MA) and stored using image acquisition software (KSA400, k-Space Associates, Inc., Ann Arbor, MI). This software controls the CCD camera exposure time, frame averaging, and conversion of measured light intensity values to gray scale levels. A neutral density filter decreases the laser power to prevent flooding of the CCD camera. The entire system is mounted on a laser table and covered by a black box to minimize stray light, dust, and air flow effects. The fluidics system includes a low-volume ( $\sim 15\text{-}\mu\text{L}$ ) flow cell, a syringe pump, two switching valves, and low dead-volume laminar flow tubing. The syringe is computer controlled using existing software for rapid time response ( $\sim 1$  s).

SPR microscopy data were collected and analyzed using the image acquisition KSA400 software. The software allows data to be collected using several modes including single image capture, multiple image movie acquisition, and a special Scan Mode. Scan Mode allows area integration (one frame of the video camera, or  $\sim 1/30$  of 1 s collection time) of the intensity in any number of preselected regions of an image, and the integrated intensity for each selected region can be averaged over a selected time window and plotted versus time.

For data acquisition using Scan Mode,  $12 \times 18$  pixel areas of the image were selected, centered on the microarray elements, by predefining "boxes" in those regions of an image of the surface collected at a high-contrast angle. Due to the incident angle, the horizontal magnification in the image is compressed by a factor of  $1/\cos \Theta$ , where  $\Theta$  is the incident angle of  $\sim 54^\circ$ . Thus, each box size corresponds to approximately  $200\ \mu\text{m} \times 200\ \mu\text{m}$  on the sensor surface. Sometimes a smaller box size was used if the spot diameter was less than  $200\ \mu\text{m}$ . The smallest box size used was  $8\ \text{pixels} \times 12\ \text{pixels}$ , corresponding to a sensor surface area of  $0.018\ \text{mm}^2$ .

To measure SPR angular curves (i.e., reflectivity versus incident angle) for all areas of interest, the reflected light intensity collected by the CCD camera was integrated for the pixels within the box as the incident/detection angles were scanned. Intensity data typically were collected at a rate of 30 Hz and time-averaged

for 1 s. Scan Mode also was used to monitor the reflected light intensity collected by the CCD camera from preselected regions of the surface during real-time adsorption and desorption measurements. For visual clarity, the contrast and brightness was adjusted for some SPR microscope images. However, all SPR curves and adsorption/desorption curves shown are composed of unfiltered intensity data. Line scans were created from normalized images made by dividing the original image by an image obtained at an angle for 100% reflectivity (no SPR) in order to eliminate the contribution of the laser beam profile.

**(2) SPR Microscopy Adsorption/Desorption Measurements.** For SPR microscopy measurements, a substrate functionalized with the microarray was removed from the storage buffer and the back of the substrate was rinsed with water and blown dry with  $\text{N}_2$ . Index-match fluid (Cargille Laboratories, Inc.) was applied to the back of the substrate, and it was mounted on the prism. The flow cell ( $\sim 15\ \mu\text{L}$ ) was mounted on the front face of the substrate/prism assembly and filled with PBS buffer. All of these steps were done quickly to minimize exposure of the microarray to dry laboratory air. All SPR microscope images were collected at a high-contrast angle in the linear region of the SPR curve for the array elements or, when possible, at an angle in the linear region for both the array elements and the surrounding surface.<sup>33</sup>

SPR microscopy adsorption experiments were done by first establishing a baseline with the microarray surface under carrier buffer (150 mM PBS buffer, pH 7.4). Then SA in the carrier buffer was injected into the flow cell. The concentration of SA in the buffer was 0.08 mg/mL unless otherwise indicated. To end adsorption, the SA solution was replaced by pure buffer.

**SPR Microscopy Data Quantitation.** The reflected intensity changes monitored by the SPR microscope were converted into surface coverages using a method for quantitation of SPR microscopy data.<sup>33</sup> This new method is an extension of the formalism described previously.<sup>34</sup> This method involves a very simple calibration of the instrumental sensitivity ( $s$ ) based on the sensor response to changes in bulk index of refraction, an exponential probe depth estimated from Fresnel equations, and the known index of refraction for the adsorbate.<sup>33,34</sup> The index of refraction for SA is 1.57<sup>34</sup> and that for DNA is 1.7.<sup>53,54</sup> A sensitivity ( $s$ ) of 3900% reflected intensity/RIU for the SPR microscope was measured by doing a calibration of the system's response to bulk changes in refractive index.<sup>33,34</sup> For clarity, RIU is used to indicate "refractive index unit", a unitless quantity. A decay length of 234 nm was calculated using previously described methods.<sup>34</sup> Specific volumes of 0.77<sup>34,55-57</sup> and 0.61  $\text{cm}^3/\text{g}$ <sup>55</sup> were used for SA and DNA, respectively.

## RESULTS AND DISCUSSION

**Microarray Fabrication.** Microarrays were fabricated using two different strategies (method 1 and method 2) that are shown schematically in Figure 3. Both methods begin with a gold surface prefunctionalized with the mixed BAT/OEG SAM and use SA as

(53) Harrington, R. E. *J. Am. Chem. Soc.* **1970**, *92*, 6957-6964.

(54) Wu, P. G.; Fujimoto, B. S.; Song, L.; Schurr, J. M. *Biophys. Chem.* **1991**, *41*, 217-236.

(55) Darnell, J. E.; Lodish, H.; Baltimore, D. *Molecular Cell Biology*; Scientific American Books: New York, 1990.

(56) Leslie, T. E.; Lilley, T. H. *Biopolymers* **1985**, *24*, 695-710.

(57) Sjölander, S.; Urbaniczky, C. *Anal. Chem.* **1991**, *63*, 2338-2345.

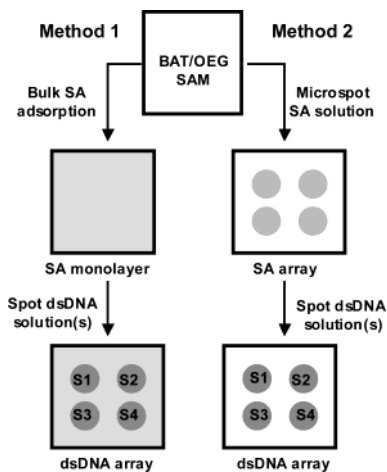


Figure 3. Schematic diagram showing the two different immobilization strategies used to fabricate dsDNA microarrays. Both methods begin with a gold-coated glass slide that is functionalized with a BAT/OEG monolayer. The next step in method 1 involves adsorption of SA to form a SA monolayer on this mixed SAM. Then dsDNA solution is spotted onto the surface using a robotic microspotting system to form a dsDNA array. The spots are labeled (S1, S2, etc.) to show the ability to immobilize dsDNAs with a unique base-pair sequence in each spot of the array. Method 2 involves using the robot to fabricate a SA array on the mixed SAM. Then a dsDNA array is created by directly spotting dsDNA solution on the SA array.

a linker layer to immobilize dsDNAs. For method 1, the next step is to form a SA monolayer by protein adsorption from solution onto the mixed SAM. Then the robotic microspotting system is used to deliver nanoliter droplets of biotinylated dsDNAs to preselected areas of the SA monolayer to create the dsDNA microarray elements.

Instead of using a preformed SA monolayer, method 2 uses the BAT/OEG SAM as the foundation for first creating a SA microarray. SA in solution is deposited by the microspotting pin on the BAT/OEG SAM to create the SA microarray. Then, a dsDNA array is created on the SA microarray by spotting biotinylated dsDNAs on top of the SA array elements. We present below the SPR microscopy characterization of microarrays fabricated using both of these methods.

**(1) dsDNA Microarray Spotted on a Uniform Streptavidin Monolayer.** A dsDNA microarray was prepared by preadsorbing SA on a BAT/OEG SAM-functionalized gold-coated substrate. Then dsDNA (0.2 mg/mL) in 400 mM PBS buffer, pH 7.4, was spotted in a  $12 \times 8$  array on this uniform SA monolayer (method 1). This array contains only two different dsDNA species, which were spotted in complete rows: a 100-mer (rows 1, 2, 5, and 6, starting from the top) and a 77-mer (rows 3, 4, 7, and 8). Figure 4 shows representative SPR reflectivity versus angle curves collected under buffer solution on and off the dsDNA spots. The SPR resonance shifts to higher angles where the DNA is present, as expected since DNA has a higher refractive index than the buffer.

Figure 5 shows a representative SPR microscope image of this dsDNA array, acquired at the high-contrast angle ( $54.44^\circ$ ) shown in Figure 4. At this angle, the DNA spots appear bright compared to the surrounding surface because of the higher reflected intensity in these areas (Figure 4). While it is possible to see the  $200\text{-}\mu\text{m}$  array elements in the image, the spot boundaries are ill-

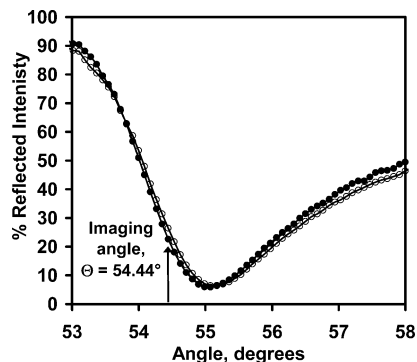


Figure 4. Representative reflectivity versus angle curves for regions of a sensor surface containing the SAM and SA (filled circles) and the SAM, SA, and dsDNA (open circles). The curves were collected with the SPR microscope for the dsDNA array fabricated on a preadsorbed SA monolayer shown in Figure 5. The curves were measured for the sensor surface under buffer for two  $0.04\text{-mm}^2$  regions of the array selected from the image in Figure 5. Each data point was measured by integrating the intensity in the selected region at a rate of 30 Hz and averaging the integrated intensity for 1 s. The curves were used to select a high-contrast angle for further SPR microscopy measurements.

defined due to the very small difference in effective refractive index caused by the addition of the DNA. A profile of the line in the image is shown in Figure 5B. The reflected intensity data (dotted line) and the data smoothed by averaging a data point at the smoothing location with the two closest neighboring data points on each side (solid line) are shown in the profile.

The amount of dsDNA in the array spots was quantitated using the intensity integration analysis method provided by the KSA software. The percent reflected intensity was integrated over a  $0.02\text{-mm}^2$  area in the center of each element of the array and in the same size area of the SA layer located just below each array element. The difference in percent reflected intensity was calculated by subtracting the intensity for the surrounding SA layer from that for the array element. These percent reflected intensity differences were averaged for each row and used to calculate the dsDNA effective thickness and packing density following the procedures outlined above. The values are shown in Table 1. The effective DNA film thickness for the 100-mer spots is systematically about one-third thicker than the 77-mer spots, consistent with their length difference. This results in much more similar dsDNA packing densities, which range from  $5 \times 10^{11}$  to  $6 \times 10^{11}$  dsDNA/cm<sup>2</sup>. The spot-to-spot standard deviations in reflected light intensity in Table 1 are much larger than the standard deviation with time within a given spot ( $\sim 0.1\%$  at one measurement per second; see below). The spot-to-spot deviation is due to spatial noise in the scattered light image, which arises from imperfections in the optics. It does not limit the instrument's sensitivity for detecting adsorption in real time within a given spot (see below).

A packing density for the SA monolayer was estimated by measuring with the SPR microscope the amount of additional SA that could be adsorbed from solution onto the areas around these dsDNA elements. These areas should contain the mixed thiol monolayer and, ideally, a saturation coverage of SA. SA (0.08 mg/mL) in 150 mM PBS buffer was allowed to adsorb to the surface, and the resulting changes in reflected intensity were measured using the SPR microscope. The average change in reflected light intensity measured for six spatially separated areas of the surface

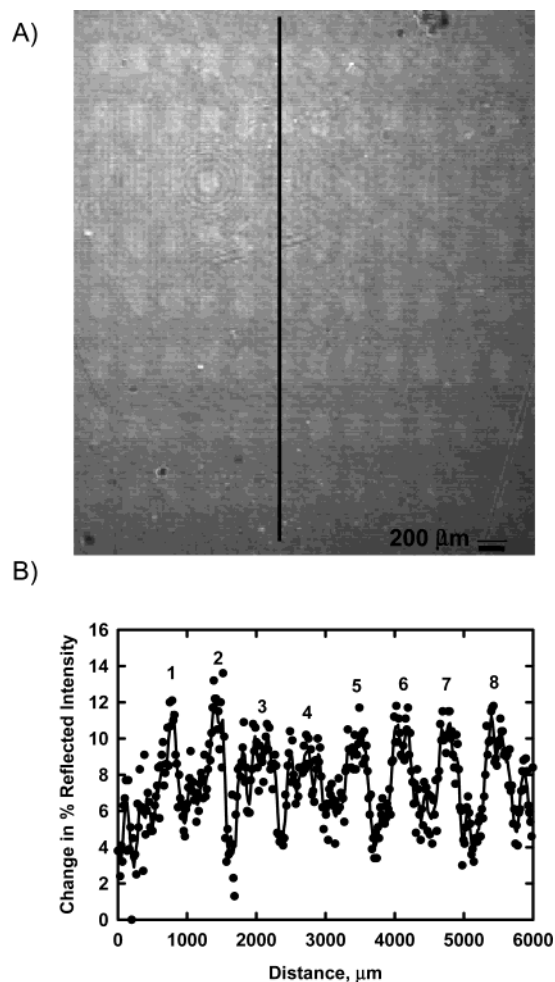


Figure 5. Microarray of dsDNA fabricated on a preadsorbed SA monolayer. (A) A high-contrast-angle SPR microscope image of the dsDNA microarray in contact with PBS buffer. (B) The profile is an average of the line profiles for a 9-pixel-wide ( $250\ \mu\text{m}$ ) column centered on the line shown in (A). Numbers indicate the row number of the array element starting from the top of the array. The solid curves in all line profiles are five-point smoothed versions of the raw data. All images are the result of averaging frames collected by the CCD camera at a rate of 30 Hz for 1 s.

was  $1.6 \pm 0.1\%$  reflected intensity. This intensity change converts to a SA effective thickness of 0.20 nm and a surface coverage of  $2.6 \times 10^{11}\ \text{SA}/\text{cm}^2$ . This is 10% of the typical SA saturation coverage of  $2.4 \times 10^{12}\ \text{SA}/\text{cm}^2$  measured on these monolayers.<sup>46,51</sup> Adsorption of this additional SA on the surface is most likely due to the binding of SA to available biotin sites left vacant due to loss of SA from the surface caused by drying of the saturated SA monolayer prior to dsDNA spotting.

If we assume the SA coverage was  $2.4 \times 10^{12}\ \text{SA}/\text{cm}^2$  prior to drying (i.e., the saturation coverage) and subtract the amount lost after drying (10%, as measured above), the estimated SA packing density at the time of dsDNA immobilization was  $2.14 \times 10^{12}\ \text{SA}/\text{cm}^2$ . The binding ratios for each of the dsDNA spots were estimated using this SA packing density and are shown in Table 1. The dsDNA/SA binding ratio of  $0.24 \pm 0.02$  is consistent for each row of the array and is somewhat below the saturation binding ratio (0.44 dsDNA/SA) measured for a similar length dsDNA adsorbed from solution onto a SA monolayer immobilized on the same composition BAT/OEG SAM.<sup>41</sup> Since each SA

exposes two biotin binding sites to the solution, only  $\sim 12\%$  of these sites are bound with the biotinylated DNA. This value of  $\sim 20\%$  observed previously was explained as due to repulsive interactions between the DNAs, preventing them from occupying nearest-neighbor biotin sites.<sup>41</sup> Since DNAs of this length are still much like rigid rods, these repulsive interactions must be electrostatic and not just due to the excluded volume of the polymer molecule.<sup>58</sup>

## (2) Streptavidin Microarray on a BAT/OEG Monolayer.

The dsDNA spotting strategy discussed above (method 1) results in low contrast in the SPR microscope images of the dsDNA microarray, making it difficult to choose the DNA areas of the image for real-time monitoring of binding events (for example, of proteins subsequently binding to these DNAs). Therefore, we next discuss the fabrication of a dsDNA array on a SA array prespotted onto the BAT/OEG SAM, method 2 in Figure 3.

The first step in this process is to microspot a SA array onto the mixed BAT/OEG SAM. An SPR microscope image of such a SA microarray acquired at a high-contrast angle is shown in Figure 6A. Each spot in the  $10 \times 12$  array is made by replicate depositions of SA solutions (0.14 mg/mL in 150 mM PBS, pH 7.4). The high contrast in the image makes it easy to see the  $200\text{-}\mu\text{m}$ -diameter SA spots. The rectangular spot shapes may be a consequence of the rectangular shape of the slit in the microspotting pin tip.

The line profile in Figure 6B shows the good signal-to-noise ratio compared to the line profile for the dsDNA fabricated on the SA monolayer shown in Figure 5B. The line profile was used to quantitate the surface coverage of SA in the spots. The difference in reflected intensity for the 10 spots is  $12.5 \pm 0.5\%$  and corresponds to an effective SA thickness of 1.6 nm. This thickness converts to a surface density of  $2.1 \times 10^{12}\ \text{SA}/\text{cm}^2$ . This is 88% of a typical saturation coverage measured by SPR for a SA monolayer on these BAT/OEG SAMs.<sup>41,46,59</sup>

The ability to fabricate a SA array with uniform coverage of SA in the individual spots is shown by the data in Table 2. The percent reflected intensity was integrated over a  $0.018\text{-mm}^2$  area in the center of each element of the array and in the same size area of a region just below each array element. The difference in percent reflected intensity was calculated by subtracting the intensity for the surrounding BAT/OEG monolayer from that for the SA array element. These percent reflected intensity differences were averaged for the spots in each row and used to calculate the SA effective thickness and packing density. The resulting values are shown in the table. A homogeneous SA surface coverage in all of the spots is shown by the low deviations for the average reflected intensity values in each row and the good agreement in the intensity values for all of the rows ( $(2.1\text{--}2.4) \times 10^{12}\ \text{SA}/\text{cm}^2$ ).

To verify the binding capacity of the BAT/OEG SAM and check whether SA coverage in the spots was at saturation, we adsorbed SA from solution to the microarray surface. Real-time SA adsorption and desorption curves measured for multiple regions of the microarray from the image in Figure 6A are shown in Figure 7. The changes in percent reflected intensity after SA was introduced to the array surface were measured by simultaneously integrating the reflected intensity at a high-contrast angle for eight spatially separated preselected  $0.018\text{-mm}^2$  areas of the

(58) Delrow, J. W.; Gebe, J. A.; Schurr, J. M. *Biopolymers* **1997**, *42*, 455–470.

(59) Jung, L. S.; Shumaker-Parry, J. S.; Campbell, C. T.; Yee, S. S.; Gelb, M. H. *J. Am. Chem. Soc.* **2000**, *122*, 4177–4184.

Table 1. Surface Coverage of dsDNAs in the Microarray in Figure 5<sup>a</sup>

array row number	dsDNA length (mer)	av diff in % reflected intensity	std dev (reflected intensity)	effective dsDNA layer thickness (nm)	surface density (10 <sup>11</sup> dsDNAs/cm <sup>2</sup> )	binding ratio (dsDNAs/SA)
1	100	3.8	1.3	0.31	5.0	0.23
2	100	3.8	1.5	0.31	5.0	0.23
3	77	2.9	1.1	0.24	4.9	0.23
4	77	2.9	2.2	0.24	4.9	0.23
5	100	3.7	1.8	0.30	4.9	0.23
6	100	4.1	1.3	0.34	5.4	0.25
7	77	3.0	1.7	0.25	5.1	0.24
8	77	3.6	1.6	0.30	6.1	0.29

<sup>a</sup> Values for percent reflected intensity were found by using Scan Mode to integrate the light intensity in a 0.02-mm<sup>2</sup> region in each array element and a region below the array element. Changes in percent reflected intensity were found by subtracting the intensity for the surrounding region from the spot intensity. A SA packing density of  $2.14 \times 10^{12}$  SAs/cm<sup>2</sup> was used to estimate the binding ratios.

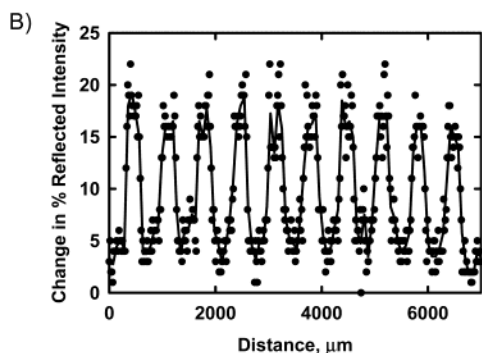
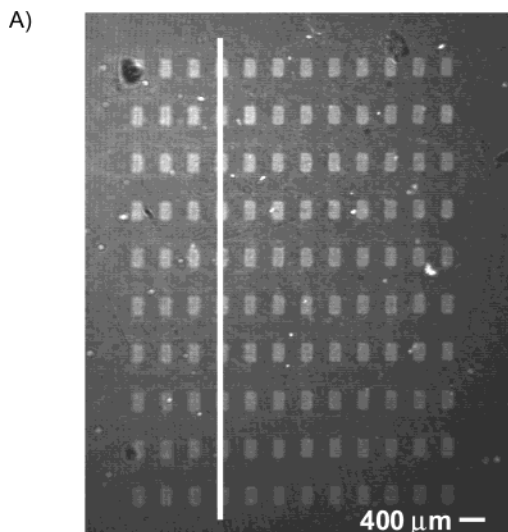


Figure 6. High-contrast-angle SPR microscope image and line profile of a SA microarray fabricated on a BAT/OEG SAM under buffer solution. (A) Rows were made by replicate SA sample depositions after a new sample uptake, (B) The profile was found by averaging the line profiles for a 4-pixel-wide column (67 μm) located in the position shown by the line in (A).

SA array. After establishing a baseline with 150 mM PBS buffer, pH 7.4, a sample of SA (0.08 mg/mL) in buffer was introduced into the flow cell. After adsorption reached saturation, the surface was rinsed with buffer. The region of the curves highlighted by the box in Figure 7A is expanded and plotted in Figure 7B. These curves demonstrate the ability to use the SPR microscopy area integration method to measure adsorption and desorption events simultaneously at many preselected regions of the surface with high sensitivity and fast time resolution (1 s). The sensitivity can be estimated from the small peak-to-peak noise on the curves:

Table 2. Surface Coverage of SA in Array in Figure 6<sup>a</sup>

array row no.	diff in % reflected intensity	std dev (% reflected intensity)	effective SA layer thickness (nm)	surface density (10 <sup>12</sup> SA/cm <sup>2</sup> )
1	12.7	1.2	1.6	2.1
2	12.9	1.7	1.6	2.1
3	13.4	1.4	1.7	2.2
4	12.9	1.5	1.6	2.1
5	12.7	1.4	1.6	2.1
6	12.6	1.3	1.6	2.1
7	14.2	0.8	1.8	2.4
8	12.9	1.3	1.6	2.1
9	13.4	0.8	1.7	2.2
10	13.0	1.1	1.7	2.2

<sup>a</sup> Values for percent reflected intensity were found by using Scan Mode to integrate the light intensity in a 0.018-mm<sup>2</sup> region in each array element and a region below the array element of the microarray. Changes in percent reflected intensity were found by subtracting the intensity for the surrounding region from the spot intensity. The reflected intensity for each row was found by averaging the values for the SA spots in that row.

$<3 \times 10^{10}$  SA/cm<sup>2</sup> or  $\sim 5 \times 10^6$  SA molecules ( $\sim 0.5$  pg of protein) in one of the spots. The curves are similar and verify the optimization of the fluidics system for rapid, simultaneous delivery of sample to all areas of the sensing surface.

An image of the surface after SA adsorption (data not shown) shows that the SA spots have disappeared after the SA adsorbed to the surrounding BAT/OEG SAM and filled in the areas between the microarray elements. The adsorption curves show a much larger increase in overall reflected intensity for the SAM than for the SA spot. The average increase in reflected intensity was  $14.8 \pm 1.1\%$  for 12 different areas on the bare thiolate monolayer between the spots and  $2.9 \pm 0.7\%$  on the 12 SA spots. These changes in percent reflected intensity correspond to effective SA thicknesses of 1.9 and 0.4 nm for the bare SAM and the SA spots, respectively. The thickness of 1.9 nm for the SA on the SAM corresponds to a surface coverage of  $2.5 \times 10^{12}$  SA/cm<sup>2</sup>. This is within 4% of a typical saturation coverage for SA on the BAT/OEG SAM.<sup>41,46,59</sup>

The thickness of 0.4 nm for the additional adsorption of SA on the SA spots corresponds to a coverage of  $5.3 \times 10^{11}$  SA/cm<sup>2</sup>. This surface coverage is  $\sim 20\%$  of a typical full SA monolayer. When this additional SA coverage is added to the initial average spot coverage measured using the line profile, the final coverage is  $\sim 2.6 \times 10^{12}$  SAs/cm<sup>2</sup>, again very close to typical saturation coverage, as expected.

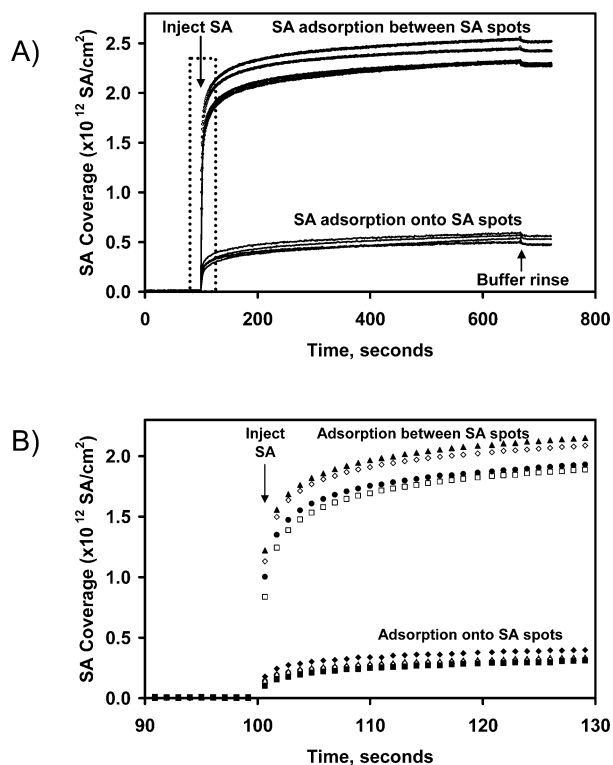


Figure 7. Real-time measurement of SA adsorption from buffer by simultaneously integrating the reflected intensity at a high-contrast angle for eight spatially separated  $0.018\text{-mm}^2$  areas of the SA array from Figure 6. The data were collected at a rate of 30 Hz and averaged for 1 s. (A) First, the baseline was established by introducing running buffer to the array surface. Then SA in running buffer was injected. As the SA adsorption approached saturation coverage, the protein sample was replaced with pure running buffer. (B) The boxed region in (A) is expanded to show this SPR microscopy technique can be used to measure adsorption and desorption events in real time for many areas simultaneously. The curves also demonstrate the optimization of the fluidics system.

The ability of additional SA to adsorb on the array spots may be due to incomplete adsorption from the solution spotted on the surface during the microspotting process. Alternatively, the additional SA may be filling sites on the BAT/OEG SAM where SA was lost due to drying. As mentioned previously, drying of the surface was minimized, but not completely eliminated. There is always some drying of the surface prior to mounting the flow cell on the substrate/prism assembly. The extent of this drying is difficult to control because it depends in part on the relative humidity in the laboratory.

The loss of SA due to drying of the microarray surface also is corroborated by the fact that the SA coverage after microspotting was 20% less than the typical saturation coverage on these mixed monolayers. When the additional SA adsorbs, the final SA coverage in the spots is within 4% of the coverage measured for the surrounding monolayer and similar to what has previously been measured.

**(3) Relationship between SA Solution Concentration and SA Surface Coverage.** To maximize the SA coverage in the microarray spots for dsDNA immobilization, we investigated the relationship between the SA solution concentration used for microspotting and the protein coverage in the microarray. SA solutions ranging in concentration from 0.46 to 0.05 mg/mL were

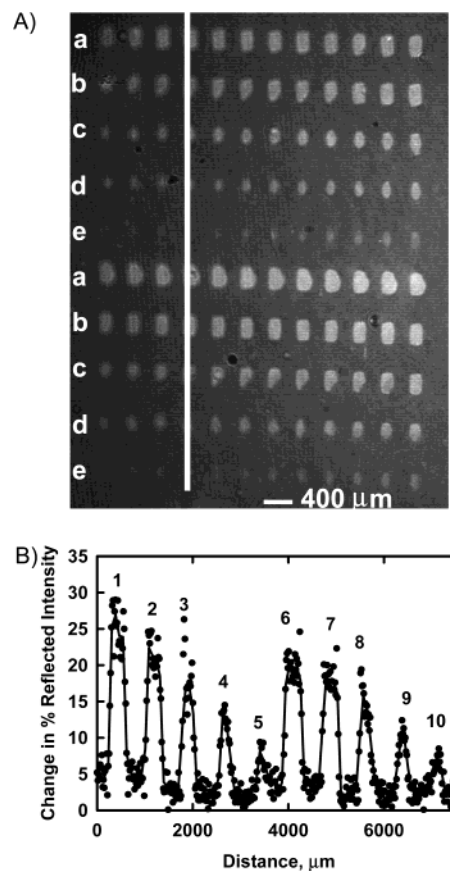


Figure 8. SPRM image and line profile for a SA microarray fabricated on a BAT/OEG SAM showing the effects of SA microspotting sample concentration. The image was acquired at a high-contrast angle with the surface in contact with PBS buffer. (A) Rows in the array represent different SA microspotting sample concentrations of (a) 0.46, (b) 0.28, (c) 0.14, (d) 0.09, and (e) 0.05 mg/mL. The elements in the row were from duplicate depositions of a single sample uptake. (B) Profile for a 4-pixel-wide ( $67\ \mu\text{m}$ ) column located in the region of the image shown by the line in (A). Numbers identify the row of the array element starting from the top of the array.

used to fabricate the SA microarray shown in the SPRM image in Figure 8A. We chose these concentrations based on the number of SA monolayers present in solution when we assume a drop delivery volume of 1.7 nL based on the specifications for our pin, a spot diameter of  $200\ \mu\text{m}$ , and a SA monolayer saturation coverage of  $2.4 \times 10^{12}\ \text{SA}/\text{cm}^2$ . The estimated number of SA monolayers contained in each droplet of each SA solution concentration is shown in Table 3.

The size and intensity of the array spots decrease for lower SA solution concentrations. The line profile in Figure 8B shows the decrease in the spot intensity for the column indicated by the line in the SPRM image. The SA coverage was calculated by measuring the difference in percent reflected intensity for the array elements using line profiles. The results were averaged for each row and are shown in Table 3. Figure 9 plots the resulting SA surface coverage within a spot versus the SA solution concentration used in spotting. Although there were several monolayers worth of SA per droplet in several of the spotting solutions according to our estimations, less than a monolayer of SA coverage was found for all of the spots. This may be due to a lower than estimated droplet volume delivered to the surface, incomplete SA adsorption from solution and its subsequent

Table 3. SA Surface Coverage for Different SA Solution Samples Used for Microspotting<sup>a</sup>

SA solution concn (mg/mL)	est no. of SA monolayers in droplet	av diff in % reflected intensity	std dev (% reflected intensity)	effective SA layer thickness (nm)	surface density ( $10^{12}$ SA/cm <sup>2</sup> )
0.46	5	12.4	1.6	1.6	2.1
0.28	3	10.4	2.0	1.3	1.7
0.14	1.5	8.8	1.9	1.1	1.5
0.09	1	6.8	1.7	0.9	1.1
0.05	0.5	3.5	1.2	0.4	0.6

<sup>a</sup> The difference in average reflected intensity relative to the surrounding regions was measured using the SPR microscope line scans for the microarray in Figure 8 in contact with PBS buffer.

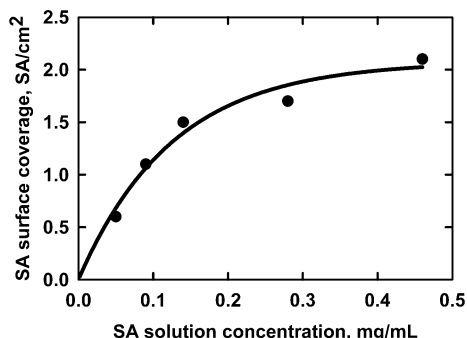


Figure 9. Relationship between the SA solution concentration for microspotting and the resulting density of SA measured in the microarray on a BAT/OEG SAM functionalized gold-coated substrate.

rinsing, or loss of SA due to drying/rinsing. This last effect could only be dominant for the highest SA concentration. The values for Table 3 and Figure 9 were obtained from line profiles rather than using intensity integration over the spot area due to the need to adjust the integration area for each spot as the spot size changed. However, to compare results obtained using both methods, we used area intensity integration for the top row of spots, which are the largest. As previously described, the reflected intensity values were found by integrating the intensity in a 0.02-mm<sup>2</sup> area centered over each spot and over an area of the BAT/OEG surface just below the spot. The difference in reflected intensity was found by subtracting the intensity value for the area below the spot from the value for the spot. The resulting intensity values were averaged for the top row of spots to give a difference in reflected intensity of  $12.0 \pm 1.3\%$ . This value agrees well with that found using the line profiles ( $12.4 \pm 1.6\%$  reflected intensity), showing that both line profiles and area integration are valid methods for measuring reflected intensity values.

#### (4) dsDNA and SA Microarray on a BAT/OEG Monolayer.

Finally, we used a SA array as the basis for immobilizing dsDNA by spotting biotinylated dsDNA directly on the array of SA spots (method 2 of Figure 3). The resulting dsDNA microarray is shown in Figure 10A. The array was made by first spotting SA (0.14 mg/mL) onto a BAT/OEG mixed monolayer. After protein was allowed to adsorb in the high-humidity chamber for 30 min, dsDNA (0.2 mg/mL) in 400 mM PBS buffer, pH 7.4, was spotted on top of the SA spots. Again, only two types of dsDNA were used: 100- (rows 2, 3, 6, and 7) and 77-mers (rows 4, 5, 8, and 9).

The top and bottom rows were spotted only with SA solution, while the other rows contain both dsDNA and SA. The high

contrast between the spots and the surrounding surface makes it easy to identify the spots and their boundaries. As expected, the reflected light intensity for the SA spots is slightly lower than that for the spots composed of SA and dsDNA. This is also shown by the line profile in Figure 10C. This is the profile for the line in Figure 10A. The amount of SA and dsDNA in the spots was quantified using line profiles. The differences in percent reflected intensity for the dsDNA spots were calculated by subtracting the average difference in percent reflectivity for the SA spots from the difference in percent reflected intensity for the spots containing dsDNA and SA. The values are presented in Table 4. The dsDNA surface density ranged from  $5 \times 10^{11}$  to  $12 \times 10^{11}$  dsDNA/cm<sup>2</sup>. The average packing density for the SA spots was  $1.7 \times 10^{12}$  SA/cm<sup>2</sup> or 70% of typical SA saturation coverage on these SAMs. This SA coverage was used to calculate the dsDNA/binding ratios shown in Table 4. The binding ratios for most of the rows are in very good agreement with those found for dsDNA immobilized on a uniform SA monolayer measured previously ( $\sim 0.4$  dsDNA/SA).<sup>41</sup> The ratios for the second and eighth array rows are slightly higher (0.74 and 0.61 dsDNA/SA, respectively), and may be due to a higher SA coverage for those rows.

SA (0.08 mg/mL) in 150 mM PBS buffer, pH 7.4, was allowed to adsorb to this dsDNA microarray. The reflected intensity changes due to SA adsorption are seen as a decrease in contrast between the spots and the surrounding area in the SPR image of the array after SA adsorption, shown in Figure 10B. It is more difficult to identify the dsDNA spot boundaries, and as expected, the DNA-free SA spots disappear completely.

The line profile for the array after SA adsorption is shown in Figure 10D. The lower signal-to-noise ratio is similar to that obtained for the dsDNA fabricated on the preadsorbed SA monolayer shown in Figure 5. The two surfaces are essentially the same at this point. The advantage of using the SA array as the basis for the dsDNA monolayer is that the spot locations (i.e., the exact pixels on the video camera image) can be identified easily prior to filling in the rest of the surface with SA. This is necessary when measuring real-time adsorption and desorption using Scan Mode, since these areas must be preselected prior to kinetic measurements.

Elsewhere,<sup>48</sup> we show that dsDNA arrays spotted by the methods outlined here can be used successfully to simultaneously monitor in real time with 1-s time resolution the binding of DNA-binding proteins to each element of the array with a sensitivity of  $\sim 0.5$  pg of protein on the spot.

**Loss of Streptavidin due to Drying.** While fabricating microarrays, we found that the treatment of the microarray surface during preparation for microspotting and prior to analysis with the SPR microscope was important for obtaining consistent high-quality arrays. Initially, we dried the substrate modified with the SA layer with N<sub>2</sub> prior to dsDNA microarray fabrication. A dry surface is necessary to prevent the droplets of DNA solutions from running together on the surface. This processing of the substrates failed to lead to reproducible dsDNA microarrays that could be observed with the SPR microscope. With SPR microscopy analysis, we measured a SA saturation coverage that was  $>25\%$  lower than that typically measured on the BAT/OEG SAM after normal adsorption from solution. We also observed adsorption of additional SA on surfaces that should already have had a saturation

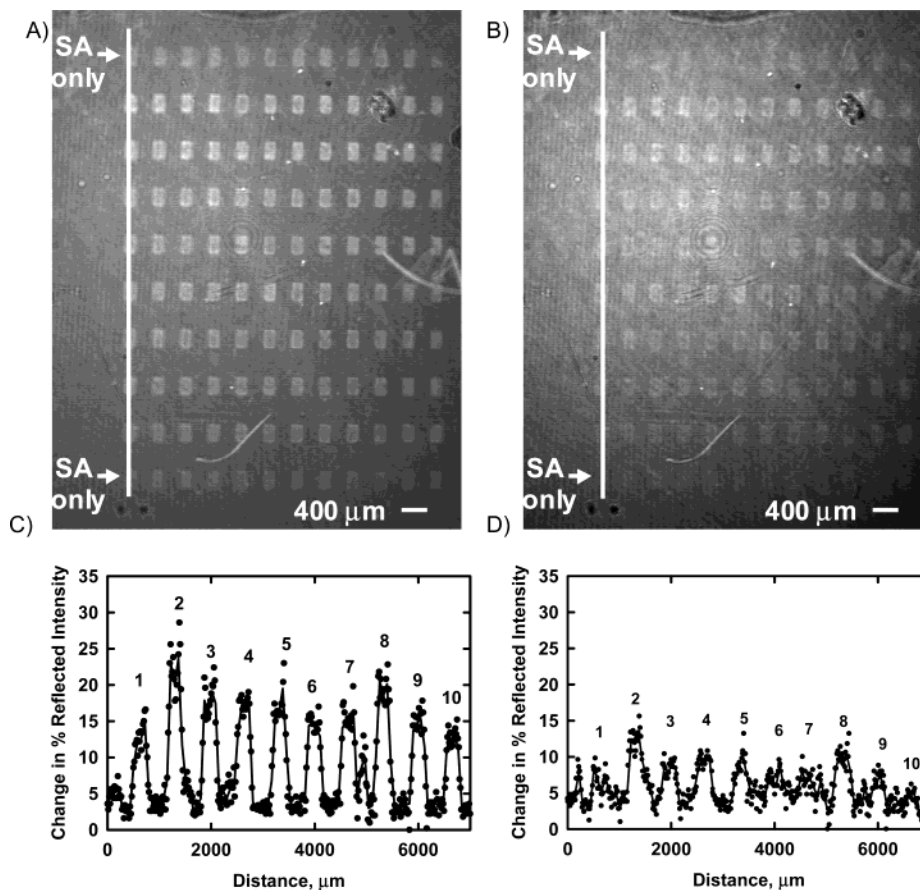


Figure 10. SPRM images and line profiles for a dsDNA microarray fabricated on a SA array on a BAT/OEG SAM. All rows contain SA. The dsDNA rows are labeled with the specific dsDNA spotted in that row. The images were acquired at a high-contrast angle with the surface in contact with PBS buffer (A) before and (B) after SA adsorption from solution. (C) Profile for the line in (A). (D) Profile of the same area as after SA adsorption from solution. Both line profiles were found by averaging the line profiles for a 9-pixel-wide ( $250\ \mu\text{m}$ ) region centered on the lines shown in the images. The curves are a five-point smoothed version of the raw data. Array elements in the line profile are labeled by the row number starting from the top of the array.

Table 4. Surface Coverages of SA and dsDNA in the Array Shown in Figure 10<sup>a</sup>

array row no.	spot compn	av diff in % reflected intensity	std dev (% reflected intensity)	diff in % reflected intensity due to dsDNAs	effective thickness (nm) of SA or dsDNA	surface density ( $10^{11}$ molecules/ $\text{cm}^2$ )	binding ratio (dsDNAs/SA)
1	SA	10.8	1.7		1.38 (SA)	18 (SA)	
2	SA+100-mer DNA	19.4	2.2	9.4	0.77	12	0.74
3	SA+100-mer DNA	16.5	1.4	6.5	0.53	8.5	0.51
4	SA+77-mer DNA	13.8	1.8	3.8	0.31	6.5	0.39
5	SA+77-mer DNA	13.5	2.4	3.5	0.29	5.9	0.36
6	SA+100-mer DNA	13.7	1.5	3.7	0.30	4.8	0.29
7	SA+100-mer DNA	14.3	2.1	4.3	0.36	5.7	0.34
8	SA+77-mer DNA	16.0	2.3	6.0	0.49	10	0.61
9	SA+77-mer DNA	13.3	1.5	3.3	0.27	5.7	0.34
10	SA	9.2	1.0		1.17 (SA)	15 (SA)	

<sup>a</sup> Differences in reflected intensity were calculated from the unsmoothed line profiles. The average of the SA packing densities for the top and bottom rows was used to estimate the binding ratios.

coverage of SA. We suspected that this apparent loss of SA from the surface was due to drying of the surfaces during microarray fabrication. We investigated this further using SPR spectroscopy and atomic force microscopy. These experiments and results are presented in ref 60.

Due to the importance of hydration to maintain a high-density and robust SA monolayer, we minimized drying of the surface

(60) Xia, N.; Shumaker-Parry, J. S.; Zareie, M. H.; Campbell, C. T.; Castner, D. G. Submitted to *Langmuir*.

between uniformly coating it with SA and microspotting biotinylated dsDNAs onto it. After adsorbing SA from solution to form a SA monolayer, the surface is rinsed with buffer and then pure water as described previously. However, rather than drying this surface with a rapid  $\text{N}_2$  flow as usual, the bulk water was instead gently blown off the surface by squirts of air from a clean squirt bottle filled with humid air from the microspotting chamber. Drying also is minimized after array fabrication by rinsing the surfaces in the high-humidity chamber and then immediately

placing the array-functionalized substrates in buffer for storage. Exposure of the substrates to the dry laboratory air is minimized prior to analysis of the microarrays with the SPR microscope. After the substrate is mounted on the prism, the flow cell is quickly fastened on top of the substrate and filled with buffer solution.

The drying effect also has relevance for storage of the slides. For the best results, the SA monolayer needs to be formed in the humid chamber just prior to microspotting. Substrates functionalized with microarrays are also stored under buffer until use. There were no obvious changes in the microarrays observed after storage under buffer for three weeks. Stability of the arrays during longer-term storage was not investigated. Elsewhere we discuss a soluble coating that allows drying the SA layers without loss of SA.<sup>60</sup>

## CONCLUSIONS

We describe here two methods for microspotting of dsDNA arrays on a gold surface. Both are based on first creating a SA layer (either uniformly across the surface or as a microspotted array) on a BAT/OEG SAM. This nearly close-packed SA layer provides  $\sim 5 \times 10^{12}$  binding sites/cm<sup>2</sup> for biotin. We showed the ability to immobilize dsDNAs on this layer so that the surface coverage of dsDNAs ( $(5-12) \times 10^{11}$  dsDNA/cm<sup>2</sup>) should allow enough space between dsDNAs for recognition and binding of DNA-binding proteins when their recognition sites are immobilized on this surface. The fabrication of a SA array with uniform coverage, followed by deposition of a biotinylated dsDNA

directly on the SA array, demonstrates the possibility of using such an SA array for the immobilization of a variety of biotinylated molecules for SPR microscopy array-based studies. We also demonstrated the ability to use the SPR microscope to measure real-time binding of protein to a patterned surface with good time resolution (1 s) and sensitivity ( $\sim 0.5$  pg of protein in a spot). The combination of such real-time adsorption and desorption SPR microscopy measurements with the SA array fabrication on the gold SPR-active surface will allow for SPR microscopy array-based studies of interactions between a variety of biomolecules with high throughput.

## ACKNOWLEDGMENT

This work was made possible by funding from the Institute for Systems Biology. J.S.S.P. thanks the University of Washington Center for Nanotechnology and its NSF IGERT program for support in the form of a graduate fellowship. We thank Dr. Leroy Hood and Dr. Krassen Dimitrov for allowing us to use the robotic microspotting system in the Institute for Systems Biology Microarraying Facility. We thank Bruz Marzolf for his assistance with the microspotting system. We thank Dr. Leroy Hood, Dr. Kjell Nelson, Dr. Nan Xia, and Bruz Marzolf for useful discussions.

Received for review August 18, 2003. Accepted November 12, 2003.

AC034964V